Further observations on the nitrogen orange afterglow

Lawrence G. Piper
Physical Sciences Inc., 20 New England Business Center, Andover, Massachusetts 01810

(Received 27 April 1993; accepted 8 September 1994)

We have extended earlier observations on the nitrogen orange afterglow that results from the excitation of $N_2(B\ ^3\Pi_g, v'=1-12)$ in the energy transfer reaction between $N_2(A\ ^3\Sigma_u^+)$ and $N_2(X, v\geq 4)$. Spectral observations out to 1550 nm show that $N_2(B, v'=0)$ accounts for about 38% of the total $N_2(B)$ excitation. This makes the rate coefficient for $N_2(B)$ excitation in the energy-transfer reaction between $N_2(A)$ and $N_2(X, v\geq 4)$ equal to $(4\pm 2)\times 10^{-11}$ cm^3 molecule^{-1} s^{-1}. Experiments involving $^{14}N_2(A)$ and isotopically labeled $^{15}N_2(X, v)$ show $^{15}N_2(B)$ is the principal product. This demonstrates that the mechanism involves electronic energy transfer from the $N_2(A)$ to the $N_2(X, v)$. The vibrational distributions of $N_2(B, v\geq 4)$ are qualitatively similar whether $^{15}N_2(v)$ or $^{14}N_2(v)$ is excited although the magnitude of $^{15}N_2(B, v\geq 4)$ excitation is about 20% larger. These distributions can be characterized roughly as a 5200 K Boltzmann distribution. In contrast, the vibronic levels of $^{14}N_2(B, v=0-2)$ are substantially more excited than are those of $^{15}N_2(B, v=0-2)$. Interestingly, the overall excitation rates for both $^{14}N_2(X, v)$ and $^{15}N_2(X, v)$ are the same to within 20%. Adding $^{14}N_2(X)$ to the mixture of $N_2(A)$ with $^{15}N_2(X, v)$ results in quenching of $^{15}N_2(B)$ and the concomitant excitation of $^{14}N_2(B)$. The rate coefficient for this electronic energy exchange reaction is $(8\pm 2)\times 10^{-11}$ cm^3 molecule^{-1} s^{-1}, about 2.5 times greater than the rate coefficient for $N_2(B)$ removal by N_2. © *1994 American Institute of Physics.*

I. INTRODUCTION

The nitrogen orange afterglow can be produced in a discharge flow apparatus by flowing dilute mixtures of nitrogen in helium or argon rapidly through a low power microwave or radio frequency discharge.[1] It has also been generated in a high voltage, low current discharge in static mixtures of nitrogen highly dilute in argon or helium.[2] This afterglow is distinctively different from the other, better known, nitrogen afterglows, the Lewis–Rayleigh (yellow), pink, blue, and green afterglows.[3,4] In common with the well-known Lewis–Rayleigh afterglow, the orange afterglow's primary emission features to the red of 500 nm are the nitrogen first-positive bands, $N_2(B\ ^3\Pi_g - A\ ^3\Sigma_u^+)$. However, the vibrational level populations of the first-positive bands in the orange afterglow decrease monotonically with increasing vibrational level, in contrast to the Lewis–Rayleigh afterglow, where the populations of vibrational levels 10–12 are elevated relative to the populations of the other vibrational levels. Generally, the N_2 B-state vibrational level populations in the orange afterglow can be characterized roughly by a 5000 K Boltzman distribution.

Spectral observations of the orange afterglow in the ultraviolet reveal the nitrogen Vegard–Kaplan bands, $N_2(A\ ^3\Sigma_u^+ - X\ ^1\Sigma_g^+)$. Ordinarily, these bands are difficult to detect in nitrogen afterglows because $N_2(A)$ has quite a long radiative lifetime,[5] about 2.5 s, and is readily quenched by nitrogen atoms.[6] Nitrogen atoms are generated in abundance in most nitrogen discharges, but flowing the gases rapidly shortens the residence time in the discharge sufficiently to reduce the production of atomic nitrogen. As a result, metastable $N_2(A)$ can persist in the flow several tens of milliseconds downstream from the discharge.

Another species abundant in the orange afterglow is highly vibrationally excited, ground-electronic-state nitrogen. Several years ago, we applied a Penning-ionization diagnostic to the orange afterglow.[7,8] This diagnostic involves introducing metastable $He(2\ ^3S)$ to the afterglow. A Penning-ionization reaction between $He(2\ ^3S)$ and vibrationally excited nitrogen results in excitation of the nitrogen first-negative bands, $N_2^+(B\ ^2\Sigma_u^+ - X\ ^2\Sigma_g^+)$. The vibrational distribution of the $N_2^+(B)$ is related to that of ground state nitrogen through the Franck–Condon factors that couple the two states. The $N_2^+(B, v)$ distribution observed in the Penning-ionization process can be inverted to give the vibrational distribution of the vibrationally excited, neutral, ground electronic state nitrogen. Our investigations showed that even a modest discharge power of 50 W was sufficient to raise more than half of the discharged nitrogen to excited vibrational levels.[8] Under certain conditions, the Penning-ionization reaction also produced some $N_2^+(C)$, thereby demonstrating the presence of ground electronic state nitrogen molecules carrying at least 3.8 eV in vibrational energy.

In a series of observations in which $N_2(A)$ and $N_2(X, v)$ were generated in separate sources and combined subsequently, we have shown that the orange afterglow is excited in an energy-pooling reaction between $N_2(A)$ and $N_2(X, v)$.[1] Exciting $N_2(B, v=1)$ requires $N_2(X, v\geq 5)$ whereas $N_2(X, v\geq 13)$ is required to generate $N_2(B, v=12)$. We have since used this energy transfer reaction to study the quenching of vibrational energy in ground electronic state nitrogen by a variety of molecules.[9]

This paper reports additional observations related to the orange afterglow. We have extended spectral observations to 1550 nm in order to quantify the contribution of emission from $N_2(B, v'=0)$ to the afterglow radiation. In addition, we have mixed isotopically labeled $^{15}N_2(X, v)$ with $^{14}N_2(A)$ to demonstrate that the excitation mechanism of the orange af-

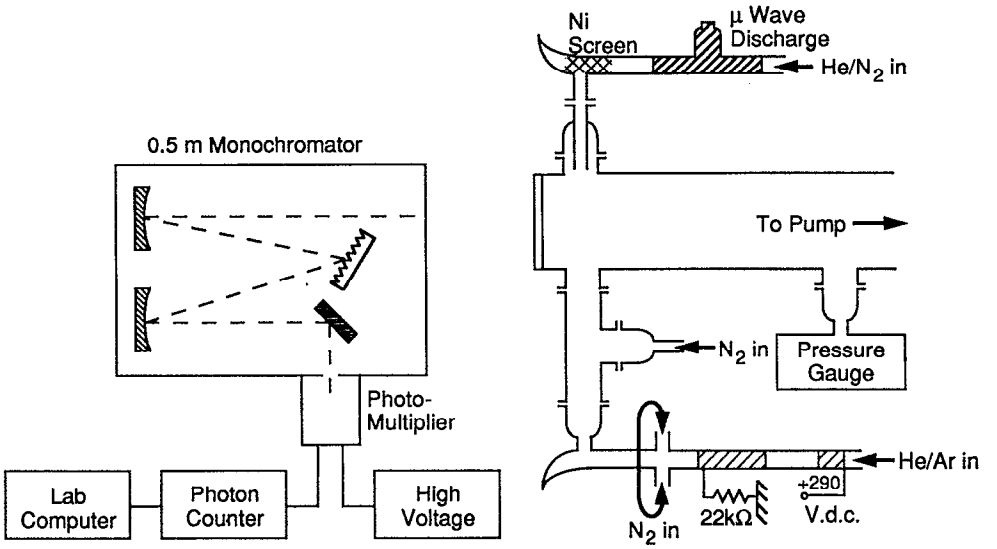

FIG. 1. Discharge-flow reactor for observing fluorescent emissions from metastable energy transfer processes.

terglow involves energy transfer from $^{14}N_2(A)$ to $^{15}N_2(X,v)$ to produce $^{15}N_2(B)$. Further, we find adding $^{14}N_2(X)$ to quench the $^{15}N_2(B)$ results in excitation of $^{14}N_2(B)$ in vibrational levels lower than those of the $^{15}N_2(B)$ initially excited.

II. EXPERIMENT

The experimental apparatus (see Fig. 1) is a 2 in. diameter discharge-flow reactor configured to allow spectral observations along the flow tube axis. The $N_2(A)$ and $N_2(X,v)$ entered the main flow reactor from opposing side arms at the reactor's upstream end. This end of the flow tube was sealed with a CaF_2 window having uniform transmission over the spectral range investigated in these studies, 200 to 1800 nm.

The $N_2(A)$ was generated by the energy transfer reaction between metastable $Ar^*(^3P_{0,2})$ and N_2.[10,11] This reaction produces $N_2(C\ ^3\Pi_u)$ which radiates immediately to the $N_2(B\ ^3\Pi_g)$ state. Subsequent radiative and collisional cascade from $N_2(B\ ^3\Pi_g)$ makes the highly metastable $N_2(A\ ^3\Sigma_u^+)$. A low-power, hollow-cathode discharge, sustained in a flow of 5% to 10% argon in helium, produces the Ar*. The N_2 then is mixed with the Ar* downstream from the discharge.

A microwave discharge sustained in a flow of 0.5% to 5% nitrogen in helium generates the $N_2(X,v)$. The discharge efflux flows through a nickel screen prior to entering the main reactor. The nickel screen removes molecular metastables other than $N_2(X,v)$ and recombines most of the nitrogen atoms produced in the discharge.[7,12]

Either mass-flow meters or rotameters measured gas flow rates. All flow meters had been calibrated either by measuring the variation of pressure with time when the gases flowed into a calibrated volume, or by comparison with a standard mass flow meter. The cylinders of nitrogen used for generating the $N_2(X,v)$ were connected to a T valve which could be rotated to admit either $^{14}N_2$ or $^{15}N_2$ into the discharge. This allowed the isotopic sources of $N_2(X,v)$ to be switched rapidly to allow comparison between the two $N_2(X,v)$ sources under otherwise similar conditions.

A 0.5 m monochromator was used to make spectral observations along the axis of the main flow tube. For measurements between 200 and 900 nm, the monochromator had a 1200 line mm^{-1} grating blazed at 250 nm. A thermoelectrically cooled HTV R943-02 photomultiplier tube, connected to a photon-counting rate meter and lab computer, detected the photons. For spectral observations between 700 and 1500 nm, the monochromator had a 300 line mm^{-1} grating blazed at 1.0 μm and a liquid nitrogen cooled, intrinsic germanium detector measured fluorescence. In the infrared measurements, light from the flow reactor was chopped prior to entering the monochromator, and a lock-in amplifier connected to the lab computer processed the signals from the intrinsic germanium detector.

The spectra observed under the various sets of conditions were analyzed using the spectral fitting procedure we have detailed previously.[13] Synthetic spectra are generated by first multiplying a set of vibronic level populations by a set of basis functions representing the intensity of a unit population of each vibronic level as a function of wavelength. The intensities of each band at each wavelength increment are then summed to determine an overall spectral intensity. A least-squares program varies the populations of each vibronic level to determine the set giving a spectrum that best matches the one observed experimentally.

The vibronic basic sets are constructed by first calculating a "stick" spectrum representing the positions and intensities of each rotational line emanating from each selected upper vibronic level. The upper state rotational populations are assumed to be in Boltzmann rotational equilibrium (300 K in the present case). The lines from each vibronic level are then convolved with a triangular slit function and their inten-

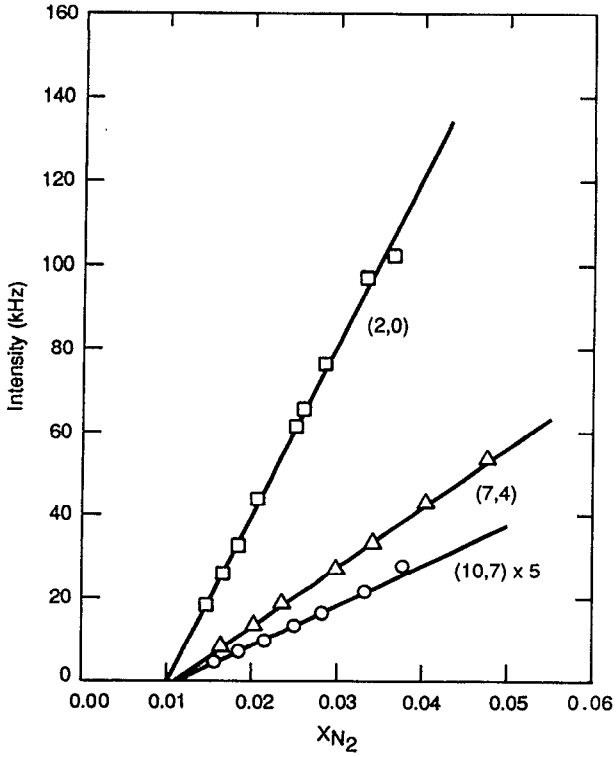

FIG. 2. Variation in the intensity of several N_2 first-positive bands excited from the interaction of $N_2(A)$ with $N_2(X,v)$ as a function of the nitrogen mole fraction in the discharge.

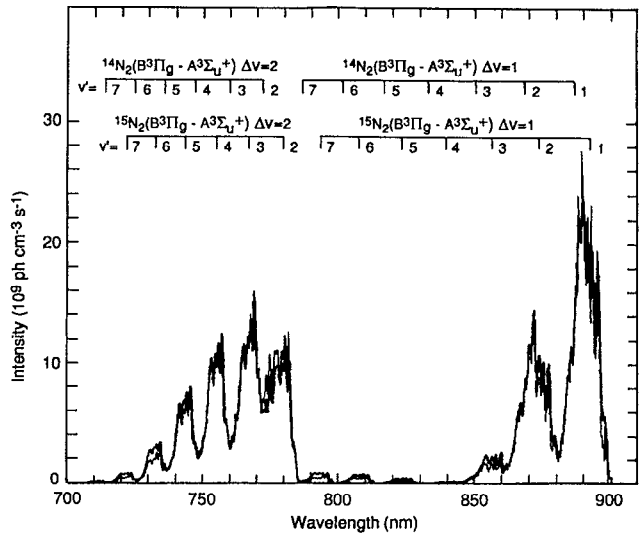

FIG. 3. Nitrogen first-positive emission between 700 and 900 nm generated from the reaction of $^{15}N_2(X,v)$ with $N_2(A)$ in the presence of 19 mTorr of $^{14}N_2(X)$. The light line is the experimental spectrum while the heavy line shows the synthetic fit to the experimental spectrum.

sities are summed at each point to give the basis sets.

The important spectral features between 200 and 400 nm were the nitrogen Vegard–Kaplan bands, $N_2(A\ ^3\Sigma_u^+ - X\ ^1\Sigma_g^+)$, nitrogen second-positive bands, $N_2(C\ ^3\Pi_u - B\ ^3\Pi_g)$, and nitric oxide gamma bands, $NO(A\ ^2\Sigma^+ - X\ ^2\Pi)$. The only significant spectral features in the visible and infrared were the nitrogen first-positive bands, $N_2(B\ ^3\Pi_g - A\ ^3\Sigma_u^+)$.

The spectral fitting procedure was essential to the analysis because emissions from $^{14}N_2(B)$ are highly overlapped with those from $^{15}N_2(B)$. Our spectra cover a number of different vibronic sequences, however, and the degree of overlap between vibronic levels in one sequence is quite different from those in the other sequences.

We used the spectroscopic constants of Roux *et al.*[14,15] or Lofthus and Krupenie[16] in generating the synthetic nitrogen spectra. Einstein coefficients for $N_2(A-X)$ were from Shemansky,[17] those for $^{14}N_2(B-A)$ from Piper *et al.*,[13] $N_2(C-B)$ from Lofthus and Krupenie,[16] and $NO(A-X)$ from Piper and Cowles.[18] We calculated a set of Einstein coefficients for $^{15}N_2(B-A)$ using the transition-moment function of Piper *et al.*[13] and a set of Franck–Condon factors that we calculated for $^{15}N_2(B-A)$ using procedures outlined previously.[19] The Einstein coefficients for $^{15}N_2(B-A)$ differed little from those for $^{14}N_2(B-A)$.

III. RESULTS

We showed previously that mixing flows of $N_2(X,v)$ and $N_2(A\ ^3\Sigma_u^+)$ generates the orange afterglow of nitrogen[1] which is characterized by nitrogen first-positive emission, $N_2(B\ ^3\Pi_g - A\ ^3\Sigma_u^+)$. Mixing $^{15}N_2(X,v)$ with $^{14}N_2(A)$ also generates the orange afterglow, but in this case the emission is predominantly from $^{15}N_2(B)$. Adding increasing amounts of vibrationally cold $^{14}N_2(X)$ to the reactor shifts the spectrum from $^{15}N_2(B)$ emission to that from $^{14}N_2(B)$. Pravilov *et al.*[20] noted similar behavior in their study on $N_2(B)$ fluorescence excited by N-atom recombination involving ^{15}N and ^{14}N.

The experimental procedure consisted of measuring nitrogen first-positive spectra generated using first $^{15}N_2(X,v)$ and then $^{14}N_2(X,v)$ as a function of the number density of added cold $^{14}N_2(X)$. This procedure allowed direct comparison of the two $N_2(X,v)$ sources at constant conditions. It also permitted extrapolation of the spectral intensities of the $^{15}N_2(B-A)$ to zero partial pressure of $^{14}N_2$. Studies between 200 and 900 nm also involved scanning the Vegard–Kaplan bands for each set of conditions to correct for variations in $N_2(A)$ number density. The experimental conditions for the infrared studies exactly matched those for the visible/UV measurements to ensure comparable number densities of $N_2(A)$ and $N_2(X,v)$.

The number densities of $N_2(X,v)$ in the observation region were deemed to vary linearly with the flow rate of N_2 in the microwave discharge. We confirmed this supposition (see Fig. 2) by observing that the intensities of several nitrogen first-positive bands increased linearly with the flow rate of nitrogen through the microwave discharge under otherwise constant conditions. This behavior is expected because the effective vibrational temperature of $N_2(X,v)$ varies little at low nitrogen mole fractions in the discharge,[8] $\lesssim 0.05$. This proportionality allowed us to normalize our observations to common conditions.

Figures 3 and 4 show how the visible spectrum of nitro-

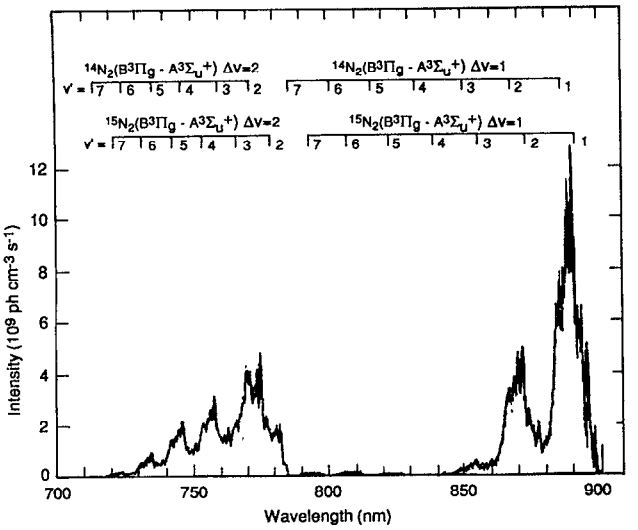

FIG. 4. Nitrogen first-positive emission between 700 and 900 nm generated from the reaction of $^{15}N_2(X,v)$ with $N_2(A)$ in the presence of 132 mTorr of $^{14}N_2(X)$.

gen first-positive bands, excited from $N_2(A)$ energy transfer to $^{15}N_2(X,v)$, changes when a substantial amount of cold $^{14}N_2$ is added to the reactor. Figures 5 and 6 show near infrared spectra under conditions similar to those of Figs. 3 and 4. The shift from primarily $^{15}N_2(B-A)$ bands at a $^{14}N_2$ partial pressure of 19 mTorr to primarily $^{14}N_2(B-A)$ bands at a $^{14}N_2$ partial pressure of 132 mTorr is particularly noticeable in the shorter wavelength spectra. The variation at longer wavelengths is more subtle, but significant enough that the spectral fitting procedure can differentiate the two isotopic emissions easily. Relative populations for $N_2(B,v=1-5)$ under constant conditions are the same whether determined from spectral scans between 500 and 900 nm or 700 and 1500 nm.

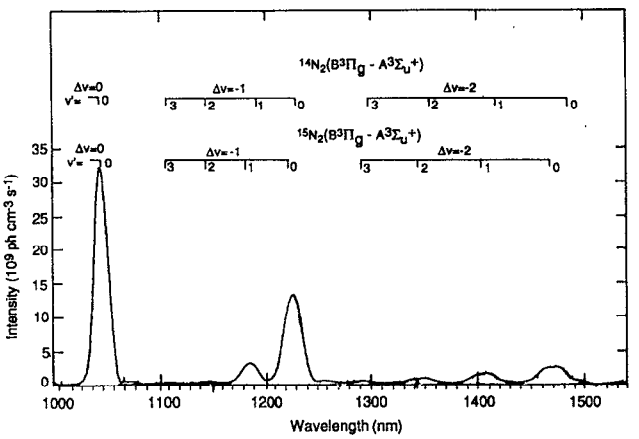

FIG. 5. Nitrogen first-positive emission between 1000 and 1500 nm generated from the reaction of $^{15}N_2(X,v)$ with $N_2(A)$ in the presence of 19 mTorr of $^{14}N_2(X)$.

The following set of reactions provides a framework for analyzing these observations:

$$N_2(A\ ^3\Sigma_u^+)+N_2(X\ ^1\Sigma_g^+,v)\rightarrow N_2(B\ ^3\Pi_g)+N_2(X,v''), \quad (1)$$

$$N_2(B\ ^3\Pi_g)\rightarrow N_2(A\ ^3\Sigma_u^+)+h\nu, \quad (2)$$

$$N_2(B\ ^3\Pi_g)+N_2\rightarrow N_2(X)+N_2, \quad (3)$$

$$^{15}N_2(B)+^{14}N_2(X)\rightarrow ^{15}N_2(X)+^{14}N_2(B). \quad (4)$$

The first three reactions can be subdivided depending upon whether $^{15}N_2(X,v)$ or $^{14}N_2(X,v)$ flows into the reactor, and will be denoted in subsequent kinetic equations by $^{15}k_1$, $^{14}k_1$, etc., when necessary.

Reaction 3, the electronic quenching of $N_2(B)$ by N_2, includes not only quenching to $N_2(X)$, but also quenching to other N_2 states such as the $A\ ^3\Sigma_u^+$ (the reverse of reaction 1), $B'\ ^3\Sigma_u^-$, $W^3\Delta_u$, and even lower vibrational levels of $N_2(B)$. Our experiments cannot distinguish these different processes. We only measure a reduction in $N_2(B-A)$ fluorescence intensity. Our previous investigations[1] demonstrated the efficacy of the reverse of reaction 1.

The rate of change in the number density of $N_2(B)$ with time is

$$\frac{d[N_2(B)]}{dt}=k_1[N_2(A)][N_2(X,v)]-\{k_2+k_3[N_2]\}\times[N_2(B)]. \quad (5)$$

This reaction is in steady state within the field of view so that the excitation and decay rates can be equated. As a result

$$[N_2(B)]=\frac{k_1[N_2(A)][N_2(X,v)]}{k_2+k_3[N_2]}. \quad (6)$$

The intensity of molecular fluorescence equals the product of the excited state number density and its radiative decay rate. As a result, Eq. (6) can be rearranged to give

$$\frac{[N_2(A)][N_2(X,v)]}{I_{N_2(B)}}=\frac{1}{k_1}+\frac{k_3}{k_1k_2}[N_2]. \quad (7)$$

A plot of the left-hand side of Eq. (7) against the N_2 number density should be linear with an intercept that is the reciprocal of the excitation rate coefficient, and a slope that is proportional to the total quenching rate coefficient.

Figures 7 and 8 show the variation in the ratio of the product of the number densities of $N_2(A)$ and $N_2(X,v)$ to the total N_2 first-positive band intensity as a function of $^{14}N_2$ number density. Figure 7 is for the excitation of vibrational levels zero through five, the near infrared data, and Fig. 8 for the visible data, vibrational levels 1 through 12. Both plots include data from $^{15}N_2(B)$ excitation and, for comparison purposes, from $^{14}N_2(B)$ excitation. The intercepts on each plot for the $^{14}N_2$ data and the $^{15}N_2$ data are essentially the same. This indicates that the total rate coefficient for $^{15}N_2(X,v)$ excitation is the same as that for $^{14}N_2(X,v)$ excitation within the limits of experimental error which are ±20%.

The ratio of the slope for $^{15}N_2(B)$ excitation to that for $^{14}N_2(B)$ excitation is the same in both Figs. 7 and 8. This

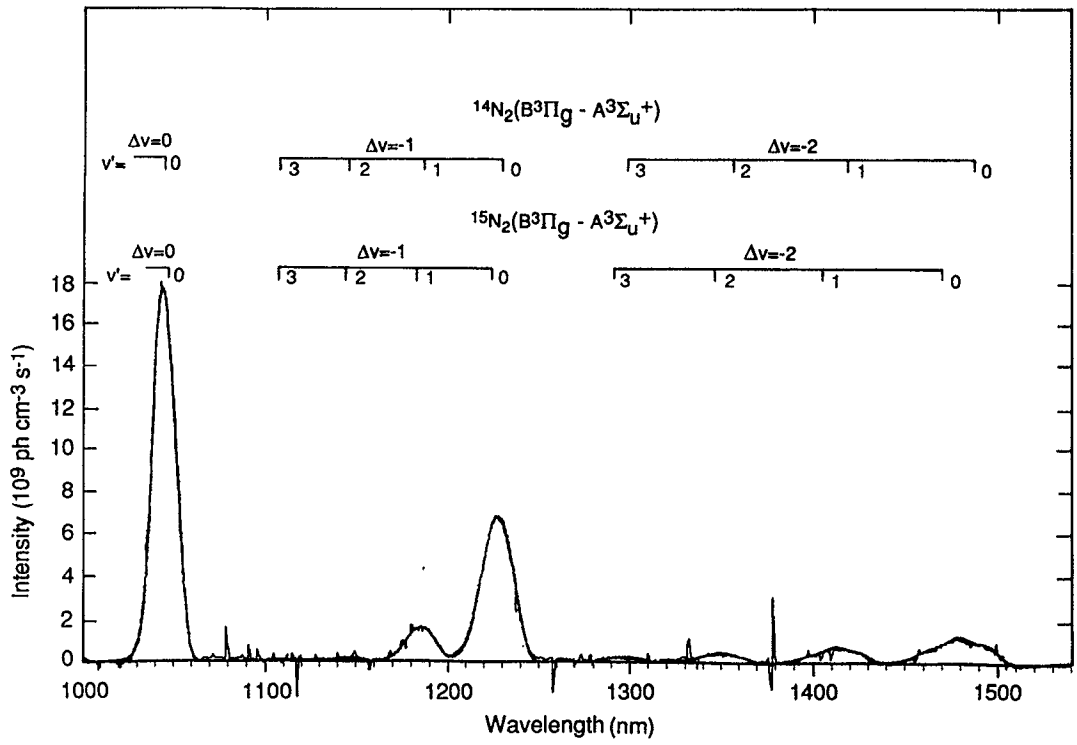

FIG. 6. Nitrogen first-positive emission between 1000 and 1500 nm generated from the reaction of $^{15}N_2(X,v)$ with $N_2(A)$ in the presence of 240 mTorr of $^{14}N_2(X)$.

ratio indicates the rate coefficient for $^{15}N_2(B)$ quenching by $^{14}N_2$ is 2.6±0.3 times greater than that for $^{14}N_2(B)$ quenching by $^{14}N_2$. We suspect that the reason for this large difference is because $^{15}N_2(B)$ can be removed not only by electronic quenching to $N_2(A)$ or $N_2(X)$, but also by energy transfer to lower vibrational levels of $^{14}N_2(B)$. While this latter process undoubtedly occurs in $^{14}N_2(B)$ as well, it is indistinguishable in our experiments from a lack of quenching.

We can determine relative rates for excitation of individual vibronic levels of $N_2(B)$ by extrapolating the reciprocal band intensities, normalized for any variations in $N_2(A)$ and total $N_2(X,v)$ number densities, to zero $^{14}N_2$ partial pressure. Figure 9 shows how the relative excitation rates vary with $N_2(B)$ vibrational level. We normalized the relative rate for $N_2(B,v'=0)$ to the others by multiplying it by the ratio of the relative rates for $N_2(B,v=1-5)$ determined in spectral scans between 500 and 900 nm to those determined from scans between 700 and 1500 nm. The relative rates for $N_2(B,v'=0)$ excitation are essentially the same for excitation from $^{15}N_2(X)$ as from $^{14}N_2(X)$ excitation, but substantial differences exist for most of the other vibrational levels. Vibrational levels 1 and 2 are excited much more efficiently from $^{14}N_2(X,v)$ than from $^{15}N_2(X,v)$, while for most of the remaining vibrational levels excitation from $^{15}N_2(X,v)$ is more efficient.

The relative excitation rates for vibrational levels $v'=4$ and above, when plotted in Boltzmann format, scale with a vibrational temperature of roughly 5200 K for both $N_2(X,v)$

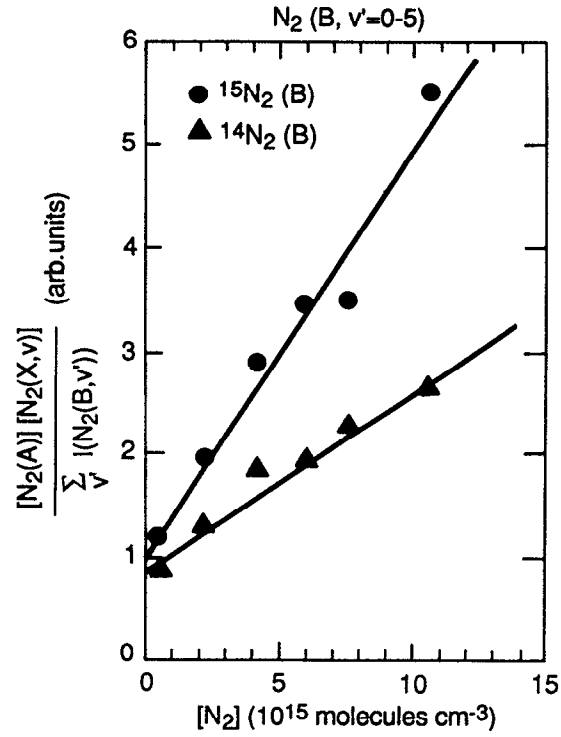

FIG. 7. Stern Volmer quenching plot for $^{15}N_2(B,v'=0-5)$ and $^{14}N_2(B,v'=0-5)$.

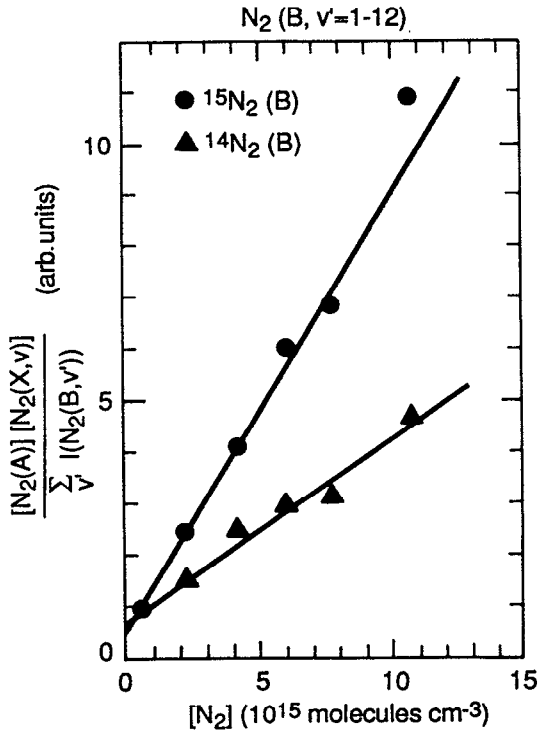

FIG. 8. Stern Volmer quenching plot for $^{15}N_2(B,v'=1-12)$ and $^{14}N_2(B,v'=1-12)$.

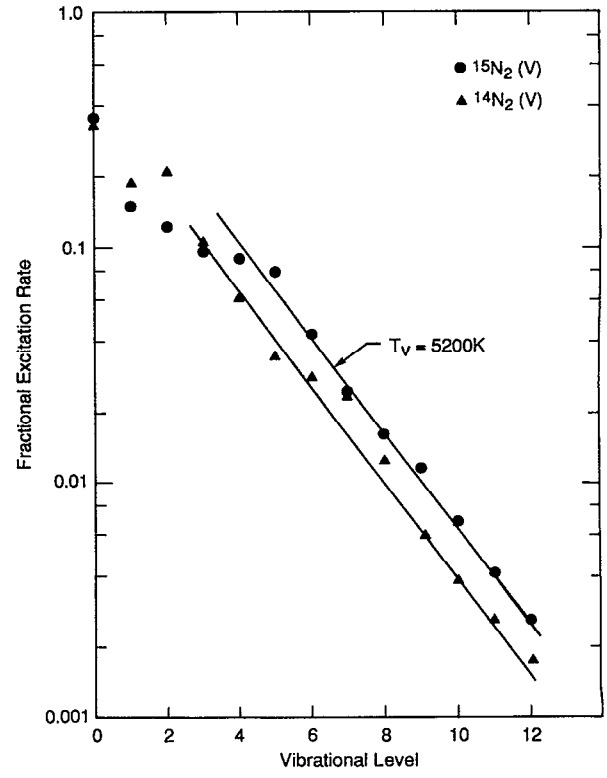

FIG. 9. Relative rates for exciting $N_2(B,v)$ in the energy transfer reaction between $N_2(A)$ and $N_2(X,v)$.

isotopes. In large part, the distribution in excitation rates with vibrational level is determined by the number densities of the $N_2(X,v)$ vibrational levels from which the $N_2(B,v)$ were excited. Thus higher $N_2(B)$ vibrational levels are excited less than the lower ones because the number densities of the $N_2(X)$ vibrational levels capable of exciting them is less. That is, $N_2(B,v'=12)$ can be excited only by $N_2(X,v\gtrsim 13)$, whereas $N_2(B,v'=0)$ can be excited by $N_2(X,v\gtrsim 4)$. We have shown previously that the $N_2(X,v)$ distribution does not follow a Boltzmann distribution, rather a modified Treanor distribution.[7,8] Interestingly, the characteristic temperature of this modified Treanor distribution is on the order of 5000 K for discharge conditions similar to those used in these studies.

In the case of $^{14}N_2(B)$ excitation by energy transfer from $^{15}N_2(B)$ to $^{14}N_2(X)$, the differential equation for the rate of change in the $^{14}N_2(B)$ number density as a function time is

$$\frac{d[^{14}N_2(B)]}{dt}=k_4[^{15}N_2(B)][^{14}N_2]-\{^{14}k_2+^{14}k_3[N_2]\}\times[^{14}N_2(B)]. \quad (8)$$

Here again, the $^{14}N_2(B)$ is in steady state so that we can equate its formation and destruction rates. Rearranging Eq. (8) gives

$$\frac{[^{15}N_2(B)]}{[^{14}N_2(B)]}=\frac{^{14}k_3}{k_4}+\frac{^{14}k_2}{k_4[N_2]}. \quad (9)$$

Figure 10 shows our data plotted in a form compatible with Eq. (9). The slope in Fig. 10 indicates that $k_4=(8.0\pm2.0)\times10^{-11}$ cm^3 molecule^{-1} s^{-1}. Multiplying this rate coefficient, i.e., k_4, by the intercept in Fig. 10 gives the rate coefficient for $^{14}N_2(B)$ quenching by N_2, $(3.2\pm0.4)\times10^{-11}$ cm^3 molecule^{-1} s^{-1}. This rate coefficient agrees nicely with other reported values for global quenching rate coefficients of $N_2(B)$ by N_2.[9,21–23] Note also that the ratio of these two rate coefficients, k_4/k_3, is 2.4 ± 0.3, the same as the ratio obtained from the analysis related to Figs. 7 and 8.

IV. SUMMARIZING REMARKS

Table I summarizes the results of this study. Initially[1] we had reported k_1 as 3×10^{-11} cm^3 molecule^{-1} s^{-1}, but subsequently revised this value upwards by 16% to correct for having discounted $N_2(B)$ quenching by CH_4.[9] Our recent revision of the $N_2(A-X)$ Einstein coefficients[5] indicates we underestimated $N_2(A)$ number densities by about 25% in our earlier study. The results of this study show that $N_2(B,v'=0)$ accounts for about 40% of the total $N_2(B)$ excitation. Incorporating this value with the two above mentioned corrections gives the total rate coefficient for excitation into all vibrational levels of $N_2(B)$, $k_1=(4\pm2)\times10^{-11}$ cm^3 molecule^{-1} s^{-1}.

Our results show that one channel for $N_2(B)$ quenching by ground electronic state nitrogen is an energy exchange reaction where molecules in higher vibrational levels of

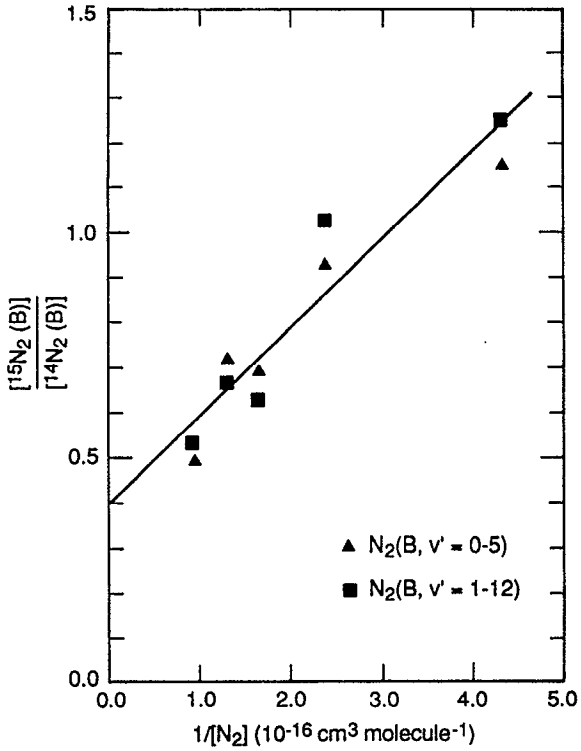

FIG. 10. Ratio of the number densities of $^{15}N_2(B)$ to $^{14}N_2(B)$ as a function of the reciprocal of the $^{14}N_2$ number density.

$N_2(B)$ transfer some of their energy to the quenching molecule exciting it to a lower B-state vibrational level. This process is in effect a form of vibrational relaxation in the B state. The apparent vibrational relaxation by N_2, in contrast to total quenching, does not appear to be all that strong, however. Vibrational distributions of $N_2(B)$ excited in processes such as N-atom recombination[24] or $N_2(A)$ energy pooling[21] appear to be relaxed only modestly at high nitrogen partial pressures, although the overall emission rates are significantly diminished. This is quite unlike the situation in an argon bath where significant distortion of the nascent $N_2(B)$ vibrational distribution from these two excitation processes is evident even at pressures as low as 1 Torr.[21,24] In this case, however, the overall band intensities diminish only slightly.

TABLE I. Rate coefficients for energy-transfer reactions involving $N_2(A\ ^3\Sigma_u^+)$, $N_2(B\ ^3\Pi_g)$, and $N_2(X\ ^1\Sigma_g^+)$.

Reaction	Rate coefficient[a]
$N_2(A) + N_2(X,v) \xrightarrow{k_1} N_2(B\ ^3\Pi_g) + N_2(X)$	4 ±2
$\frac{k_1(^{15}N_2(X,v))}{k_1(^{14}N_2(X,v))}$	1.0±0.2
$^{15}N_2(B) + {}^{14}N_2(X) \rightarrow {}^{14}N_2(B) + {}^{15}N_2(X)$	8 ±2
$^{14}N_2(B) + N_2(X) \rightarrow 2N_2(X)$ or $N_2(A) + N_2(X)$	3.2±0.4

[a]Units of rate coefficients are 10^{-11} cm^3 molecule^{-1} s^{-1}.

Another product channel for $N_2(B)$ quenching by N_2 will be the reverse of reaction 1, i.e., the production of $N_2(A)$ and $N_2(X,v)$. This undoubtedly is the major pathway by which nitrogen that is excited by metastable argon energy transfer[10,11] is channeled into the A state. Metastable argon excites $N_2(C\ ^3\Pi_u)$ which radiates to $N_2(B\ ^3\Pi_g)$ in about 40 ns.[16] However, further radiative cascade from $N_2(B)$ to $N_2(A)$ via first-positive emission is too slow to compete with collisional processes at normal nitrogen partial pressures downstream from a metastable argon producing discharge. Thus the $N_2(A)$ must be produced predominantly by collisional processes. It is not coincidental, therefore, that our measured rate coefficients for reaction 1 and its reverse (essentially reaction 3) are identical.

Since the completion of this work, Bachmann *et al.* have published detailed studies on the collisional coupling of the $A\ ^3\Sigma_u^+$, $B\ ^3\Pi_g$, and $W\ ^3\Delta_u$ triplet states of N_2.[25,26] Subsequent investigations by Ottinger *et al.*[27,28] focused on the collisional coupling between the $A'\ ^5\Sigma_g^+$ and $B\ ^3\Pi_g$ states. They used a molecular beam apparatus so that they could study the coupling processes under single collisional conditions. Their primary diagnostic was fluorescence in the first-positive system, excited by radiative cascade from the $N_2(W)$ state, or collisions between A- and W-state molecules in the molecular beam and various additive gases. The collisions took place either in a collision cell that could be placed at various distances from the excited nitrogen beam source or in a crossed beam. In addition they observed perturbations in the collision-induced afterglow when various vibrational levels of the $N_2(A)$ state were pumped optically. They analyzed their observations to determine detailed state-to-state cross sections for many of the coupling processes. They found that the basic collisional coupling was strongest between levels in close energy resonance. They parametrized their results with a basic energy-gap model,

$$\sigma = \sigma_0 \exp(-|E|/E_0), \tag{10}$$

where σ_0 and E_0 are a characteristic cross section and energy for each of the gases and reservoir states studied.

In contrast to these microscopic investigations, our observations provide a more global description of energy-transfer processes in excited nitrogen systems, i.e., a description of the behavior of a highly collisionally coupled system. As such, they provide a more representative picture of overall behavior of excited nitrogen in discharges, disturbed atmospheres, laser systems, etc. Ultimately, of course, one should be able to reconcile global observations in terms of a detailed state-to-state mechanism.

Our observations lack sufficient detail to warrant their meticulous modeling using the cross sections reported by Bachmann *et al.* However, even a superficial comparison is enlightening. By applying the principal of microscopic reversibility, we used Bachmann *et al.*'s σ_0 and E_0 to calculate a set of cross sections for coupling, by collisions with N_2, the various B-state vibrational levels to those levels of the A and W states most nearly in resonance with them. Multiplying these cross sections by the mean thermal velocity of a collision between two nitrogen molecules resulted in a set of collisional coupling rate coefficients. The total effective

B-state quenching rate coefficients are then the sum of the individual rate coefficients for coupling to the A and W states. The rate coefficients for vibrational levels 0 to 11 were constant to within 25% with a mean value of 3.7×10^{-11} cm^3 molecule^{-1} s^{-1}. This value compares quite favorably with our determination above of k_3. A more detailed comparison would involve developing a model that included the appropriate back reactions. The net effect of the back reactions would be to reduce the effective B-state quenching rate coefficients slightly.

ACKNOWLEDGMENTS

We appreciate partial financial support from the Air Force Office of Scientific Research (Task 2310G4) and the Defense Nuclear Agency (Project SA, Task SA/SDI, work unit 00175) through a contract with the Phillips Laboratory, Geophysics Directorate, F19628-88-C-0173.

[1] L. G. Piper, J. Chem. Phys. **91**, 864 (1989).
[2] C. Kenty, *Proceedings of the 3rd International Conference on Physics of Electronic and Atomic Collisions*, edited by M. C. R. McDowell (North-Holland, Amsterdam, 1964), p. 1133.
[3] A. N. Wright and C. A. Winkler, *Active Nitrogen* (Academic, New York, 1968).
[4] O. Oldenberg, J. Opt. Soc. Am. **61**, 1092 (1971).
[5] L. G. Piper, J. Chem. Phys. **99**, 3174 (1993).
[6] L. G. Piper, J. Chem. Phys. **90**, 7087 (1989).
[7] L. G. Piper and W. J. Marinelli, J. Chem. Phys. **89**, 2918 (1988).
[8] L. G. Piper, K. Donohue, W. J. Kessler, T. R. Tucker, W. P. Cummings, W. J. Marinelli, and S. J. Davis, "Laser Based Diagnostics for $N_2(X,v)$," Contract F-29601-87-C-0056. Available through NTIS as WL-TR-90-45 (1990); L. G. Piper and W. P. Cummings, manuscript in preparation.
[9] L. G. Piper, J. Chem. Phys. **97**, 270 (1992).
[10] D. H. Stedman and D. W. Setser, Chem. Phys. Lett. **2**, 542 (1968).
[11] D. W. Setser, D. H. Stedman, and J. A. Coxon, J. Chem. Phys. **53**, 1004 (1970).
[12] L. G. Piper, J. Phys. Chem. **95**, 3965 (1991).
[13] L. G. Piper, K. W. Holtzclaw, B. D. Green, and W. A. M. Blumberg, J. Chem. Phys. **90**, 5337 (1989).
[14] F. Roux, D. Cerny, and J. Verges, J. Mol. Spectrosc. **97**, 302 (1982).
[15] F. Roux and F. Michaud, J. Mol. Spectrosc. **116**, 43 (1986).
[16] A. Lofthus and P. Krupenie, J. Phys. Chem. Ref. Data **6**, 113 (1977).
[17] D. E. Shemansky, J. Chem. Phys. **51**, 689 (1969).
[18] L. G. Piper and L. M. Cowles, J. Chem. Phys. **85**, 2419 (1986).
[19] W. J. Marinelli and L. G. Piper, J. Quant. Spectrosc. Radiat. Transfer **34**, 121 (1985).
[20] A. M. Pravilov, L. G. Smirnova, and A. F. Vilesov, Chem. Phys. Lett. **144**, 469 (1988).
[21] L. G. Piper, J. Chem. Phys. **88**, 6911 (1988).
[22] D. E. Shemansky, J. Chem. Phys. **64**, 565 (1976).
[23] R. A. Young, T. G. Slanger, and G. Black, J. Chem. Phys. **50**, 303 (1969).
[24] R. L. Brown, J. Chem. Phys. **52**, 4064 (1970).
[25] R. Bachmann, X. Li, Ch. Ottinger, and A. F. Vilesov, J. Chem. Phys. **96**, 5151 (1992).
[26] R. Bachmann, X. Li, Ch. Ottinger, A. F. Vilesov, and V. Wulfmeyer, J. Chem. Phys. **98**, 8606 (1993).
[27] Ch. Ottinger, L. G. Smirnova, and A. F. Vilesov, J. Chem. Phys. **100**, 4848 (1994).
[28] Ch. Ottinger and A. F. Vilesov, J. Chem. Phys. **100**, 4862 (1994).